LANGMUIR Article
Cite This: Langmuir 2019, 35, 5975−5986
pubs.acs.org/Langmuir

Bottom-Up Approach to the Coarse-Grained Surface Model: Effective Solid−Fluid Potentials for Adsorption on Heterogeneous Surfaces

Kaihang Shi, Erik E. Santiso,* and Keith E. Gubbins*

Department of Chemical & Biomolecular Engineering, North Carolina State University, Raleigh, North Carolina 27606, United States

Supporting Information

ABSTRACT: Coarse-grained surface models with a low-dimension positional dependence have great advantages in simplifying the theoretical adsorption model and speeding up molecular simulations. In this work, we present a bottom-up strategy, developing a new two-dimensional (2D) coarse-grained surface model from the "bottom-level" atomistic model, for adsorption on highly heterogeneous surfaces with various types of defects. The corresponding effective solid−fluid potential consists of a 2D hard wall potential representing the structure of the surface and a one-dimensional (1D) effective area-weighted free-energy-averaged (AW-FEA) potential representing the energetic strength of the substrate−adsorbate interaction. Within the conventional free-energy-averaged (FEA) framework, an accessible-area-related parameter is introduced into the equation of the 1D effective solid−fluid potential, which allows us not only to obtain the energy information from the fully atomistic system but also to get the structural dependence of the potential on any geometric defect on the surface. Grand canonical Monte Carlo simulations are carried out for argon adsorption at 87.3 K to test the validity of the new 2D surface model against the fully atomistic system. We test four graphitic substrates with different levels of geometric roughness for the top layer, including the widely used reference solid substrate Cabot BP-280. The simulation results show that adding one more dimension to the traditional 1D surface model is essential for adsorption on the geometrically heterogeneous surfaces. In particular, the 2D surface model with the AW-FEA solid−fluid potential significantly improves the adsorption isotherm and density profile over the 1D surface model with the FEA solid−fluid potential over a wide range of pressure. The method to construct an effective solid−fluid potential for an energetically heterogeneous surface is also discussed.

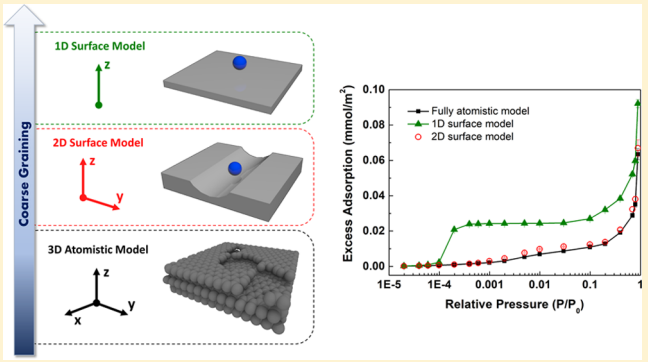

INTRODUCTION

Adsorption on heterogeneous surfaces has been intensively and extensively studied in experiments, computer simulations, and theories. In computer simulations, the surface heterogeneity can be easily introduced by removing solid atoms from the surface[1−3] to create geometric defects or by adding heteroatom or functional groups to create energetic defects;[4,5] such treatments require the solid−fluid potential with full positional dependence. However, in theoretical treatments, the solid−fluid potential with full positional dependence will make analytical and numerical calculations complicated and often intractable. The use of an effective solid−fluid potential, which has only one- or two-dimensional (1D or 2D) positional dependence reduces the complexity of the theory. Efforts have been made in density functional theory (DFT) methods[6−9] to model the heterogeneous surfaces. The quenched solid density functional theory (QSDFT) method[7,10] is formulated in the case of geometrically heterogeneous solid media. The QSDFT models the solid using the density distribution of solid atoms in the z-direction (the direction perpendicular to the surface) rather than the source of the external potential field. In particular, the two-dimensional nonlocal density functional theory (2D-NLDFT)[8,11] considers both geometrically and energetically heterogeneous surfaces. The theory uses a two-dimensional periodic function together with a modified 10-4-3 Steele potential to model the corrugation and energetic heterogeneity of the surface. These DFT methods use a very general substrate model, which has limited relation to the real atomic substrate counterpart, and the parameters in the solid−fluid potential are fitted to the "top-level" experimental adsorption data. We call such a potential construction procedure as "top-down" strategy, namely, obtaining the energy and structure information of the substrate from the experimental data. Although the top-down strategy would lead to a satisfactory reproduction of the experimental data, it loses

Received: February 14, 2019
Revised: April 1, 2019
Published: April 8, 2019

DOI: 10.1021/acs.langmuir.9b00440
Langmuir 2019, 35, 5975−5986

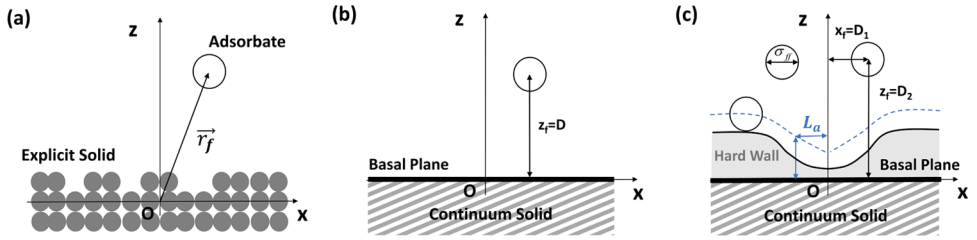

Figure 1. Schematic plots of adsorbate particles near a solid wall. (a) Three-dimensional fully atomistic model (*y*-direction is perpendicular to the *xz*-plane) with a heterogeneous substrate (composed of gray particles), where the fluid particle's position is described by a three-dimensional vector $\vec{r}_f$. (b) Typical 1D coarse-grained surface model used by Forte et al.,[23] where the heterogeneous substrate is mapped to a 1D continuum (structureless) solid with a flat surface; the corresponding effective solid−fluid potential only depends on the vertical distance of the fluid particle to the basal plane at $z = 0$. (c) New 2D coarse-grained surface model developed in this work. The coarse-grained heterogeneous substrate is composed of two parts: a 1D continuum solid with a basal plane at $z = 0$ and a 2D hard wall (gray area) at $z > 0$. The total solid−fluid potential now depends on the *x*-position of the fluid particle (parallel to the basal plane), as well as its vertical distance to the basal plane. The hard wall is inaccessible to the whole fluid particles whose diameter is determined by the Lennard-Jones (LJ) size parameter σ_{ff}. The configuration of the hard walls is characterized by an accessible length L_a, and the hard wall is symmetric about the axis $x = 0$. See the text for details.

the direct connection to the details of the substrate at a molecular level.

In contrast to the top-down strategy, for a given atomic substrate, an analytical expression of the effective solid−fluid potential for the corresponding surface structure can be found by integration over all solid atoms, which we refer to as the "bottom-up" strategy. Early attempts were the Crowell−Steele 10-4 potential[12] for the simple nonpolar molecules interacting with a semi-infinite graphite lattice and the more accurate Steele 10-4-3 potential[13] for a solid with equally spaced layers. To model simple heterogeneous surfaces, Bojan and Steele developed an analytical two-dimensional solid−fluid potential for graphite with a pair of straight-edged ledges onto a flat surface[14,15] and with stacks of graphite basal planes truncated to form an infinite set of steps of constant width and height.[16] More recently, Zhao et al.[17] developed an effective solid−fluid potential, including dipole-induced dipole, dipole−quadrupole and quadrupole−quadrupole interactions, for strongly polar molecules adsorbing on a planar graphite surface. Efforts have also been made on more complicated well-defined pore geometries, including cylindrical and spherical pore geometries,[18] truncated cone shape,[19] and overlapping spherical pore geometries.[20,21] Liu et al.[22] summarized the analytical expressions for solid−fluid potentials of a total of 19 solid models: layers and solids of different geometries (triangle, slab, cylinder, and sphere) and different dimensionalities (infinite, semi-infinite, and finite). These integrated solid−fluid potentials correspond to a simple average of the sum of the pair interactions of a fluid molecule with the solid atoms. Forte et al.[23] have shown that these integrated potentials are the leading-order term in the high-temperature expansion of the free-energy-averaged (FEA) solid−fluid potential. They concluded that the use of integrated solid−fluid potentials, such as the (10-4) potential, should be restricted to relatively high-temperature conditions, where kinetic energy is dominant and the intricate details of the surface (e.g., gaps) are not important for the adsorption. In the special case of graphite, because the surface is so compact and smooth, the use of the (10-4-3) potential leads to negligible deviations from the FEA potential even at low temperatures. For more loosely packed surfaces, or for surfaces with irregular geometrical defects, the temperature-dependent FEA potential was shown to be highly preferable to the simple average of the configuration energy of a fluid molecule with the solid substrate.[23]

The FEA solid−fluid potential is obtained by mapping the free energy of the coarse-grained system to that of the full system. Although the free-energy-averaged method has been widely employed to derive orientation-independent or angle-averaged fluid−fluid interactions in perturbation expansions,[24,25] its extension to solid−fluid interactions has been generally overlooked. The current one-dimensional (1D) effective FEA solid−fluid potential has two major limitations:

(1) It does not work well for surfaces with large geometrical defects. The FEA solid−fluid potential overestimates the density of the adsorbed fluid at pressures close to saturation. Forte et al.[23] explained it as a consequence of assuming fluid−fluid interactions to be independent of the adsorption. One way to take fluid−fluid interactions into account is to have multiple effective solid−fluid potentials at different pressures.[6] At low pressures, the solid−fluid potential is expected to have a "deep" potential well to account for those active vacancies in the surface, whereas at high pressures, the solid−fluid potential should have a "shallow" potential well, because those active sites on the surface have already been taken by preadsorbed fluid molecules and subsequent increase in the adsorption amount only involves weaker surface sites. The use of multiple effective solid−fluid potentials is possible in practice but inconvenient. Khlyupin and Aslyamov[9,26] developed an effective solid−fluid potential in the framework of a randomly rough surface. They explicitly incorporate the free space available to the fluid particle near the surface into their DFT formulation, but their construction of the effective solid−fluid potential is still limited to the leading-order term in the high-temperature expansion of the FEA potential, which is known to be inaccurate at low temperatures. In this work, we propose a simpler and more transferable approach to all types of geometrically defective surfaces. We introduce an additional parameter related to the accessible area of the geometric vacancies on the surface; a new two-dimensional (2D) surface model can then be developed consisting of a 2D hard wall potential that depends on the vertical distance from the surface (*z*-direction) and on the position parallel to the surface (*x*-direction), and a one-dimensional (1D) area-weighted free-energy-averaged (AW-FEA) energetic potential, which only depends on the vertical distance to the

DOI: 10.1021/acs.langmuir.9b00440
Langmuir 2019, 35, 5975−5986

surface. This new coarse-grained surface model contains both the energetic and structural information of the full interfacial system. Grand canonical Monte Carlo (GCMC) simulations are performed to test the validity of our 2D surface model against the fully atomistic model.

(2) It is not flexible enough for energetically heterogeneous surfaces. We need to reevaluate the effective solid−fluid potential every time for the specific surface structure, with the variation of energetic site densities. Here, we consider the recently developed conformal sites theory[4] for adsorbed layers on heterogeneous surfaces, and we briefly outline such an approach in the Appendix.

THEORY AND SIMULATION DETAILS

Coarse-Grained Description of Solid−Fluid Interactions for Geometrically Heterogeneous Surface Model. The general idea of constructing a coarse-grained (CG) surface model is to map a fully atomistic solid−fluid interaction potential to a coarse-grained effective solid−fluid potential, as illustrated in Figure 1. The full solid−fluid (sf) interaction potential U_{sf}^{full} in Figure 1a is a function of the particle's position in the system; the calculation of such a potential is the summation of the interaction energy of N_f fluid (f) particles with all N_s solid (s) atoms

$$U_{sf}^{full}(\mathbf{r}_s^{N_s}, \mathbf{r}_f^{N_f}) = \sum_i^{N_s} \sum_j^{N_f} u(r_{ij}) \tag{1}$$

where $\mathbf{r}_s^{N_s} \equiv \mathbf{r}_{s1}, \mathbf{r}_{s2}, ..., \mathbf{r}_{sN_s}$ and $\mathbf{r}_f^{N_f} \equiv \mathbf{r}_{f1}, \mathbf{r}_{f2}, ..., \mathbf{r}_{fN_f}$ are shorthand notations of positions of all solid atoms and all fluid particles, respectively; $u(r_{ij})$ is the pairwise potential energy between solid atom i and fluid particle j with distance r_{ij}. This full potential is usually applied in the molecular dynamics and Monte Carlo simulations, the evaluation of which could be very expensive if the system is large.

Figure 1b shows a typical 1D coarse-grained surface model where the atomistic substrate is represented by a continuum (structureless) solid with a flat surface; the continuum solid is uniform in both x- and y-directions and shows energetic dependence only in the z-direction. Thus, the corresponding solid−fluid interaction potential is only a function of the vertical distance of a fluid particle to the surface. When applying the free-energy-averaged method, the evaluation of the total solid−fluid interaction energy U_{sf}^{FEA} for this CG model now requires the summation of all N_f adsorbate molecules, and the positional dependence of the potential reduces from three dimensions (i.e., x-, y-, and z-directions) to one dimension (i.e., z-direction)

$$U_{sf}^{FEA}(z_{f1}, z_{f2}, ..., z_{fN_f}) = \sum_i^{N_f} \phi_{FEA}(z_{fi}) \tag{2}$$

where ϕ_{FEA} represents the effective FEA solid−fluid potential compatible with the 1D surface model. This treatment of the solid−fluid potential greatly simplifies the theoretical treatment of a complex interfacial system and speeds up the molecular simulations. However, it has been confirmed that the FEA solid−fluid potential overestimates the adsorption amount for the geometrically heterogeneous surface when substrate atoms are loosely packed or missing, creating vacancies and corrugations to the surface.[23]

To improve the performance of the effective solid−fluid potential in a system where the solid surface contains geometric defects, we developed a new coarse-grained surface model shown in Figure 1c. The coarse-grained substrate now is composed of a 1D structureless solid with a basal plane at $z = 0$ similar to that in Figure 1b and a 2D hard wall, which is uniform only in the y-direction (perpendicular to the paper) and shows the variations in both x- and z-directions. The hard wall is symmetric about the axis $x = 0$ and is inaccessible to the whole fluid particle characterized by the Lennard-Jones diameter of σ_{ff}. The purpose of constructing this hard wall is to mimic the geometric defects in the surface. If we imagine that a fluid particle is rolling over the hard wall surface, the blue dashed line in Figure 1c is the locus of its center of mass; this locus essentially determines the configuration of the hard wall. We can use a single parameter, accessible length L_a, to describe the shape of this locus. The total solid−fluid interaction potential then is given by

$$U_{sf}^{AW\text{-}FEA}(x_{f1}, x_{f2}, ..., x_{fN_f}, z_{f1}, z_{f2}, ..., z_{fN_f}) = \sum_i^{N_f} [\phi_{Hard}(x_{fi}, z_{fi}) + \phi_{AW\text{-}FEA}(z_{fi})] \tag{3}$$

where $\phi_{AW\text{-}FEA}$ is the energetic part of the total potential $U_{sf}^{AW\text{-}FEA}$ and $\phi_{Hard}(x_{fi}, z_{fi})$ is the 2D hard wall potential representing the structural part of the total potential

$$\phi_{Hard}(x_{fi}, z_{fi}) = \begin{cases} 0 & |x_{fi}| < L_a(z_{fi}) \\ +\infty & |x_{fi}| \geq L_a(z_{fi}) \end{cases} \tag{4}$$

whose configuration is determined by the accessible length parameter L_a. The energetic part of the total potential, $\phi_{AW\text{-}FEA}$, is still constructed within the free-energy-averaged framework, but now it comes with an additional parameter related to the accessible area close to the surface. We denote this potential $\phi_{AW\text{-}FEA}$ as the effective area-weighted free-energy-averaged (AW-FEA) solid−fluid potential. The next question is how can we relate this 2D coarse-grained surface model to the corresponding atomistic system?

We consider a solid substrate consisting of N_s solid atoms of the same kind with fixed positions, as illustrated in Figure 1a. Thus, interactions between pairs of solid atoms are neglected. In the canonical ensemble, the full partition function of a single fluid particle (i.e., $N_f = 1$) interacting with this solid substrate at temperature T can be written as

$$Q_{full} = \frac{1}{\Lambda^3} \int \exp\left(-\frac{U_{sf}^{full}(\mathbf{r}_s^{N_s}, \mathbf{r}_f)}{k_B T}\right) d\mathbf{r}_f \tag{5}$$

where $\Lambda = (h^2/2\pi m k_B T)^{1/2}$ is the de Broglie thermal wavelength, k_B is the Boltzmann constant, and $\mathbf{r}_s$ and $\mathbf{r}_f$ are the positional vectors for the solid atom and the fluid particle, respectively. The integration in eq 5 is over the whole phase space or simulation box. If the single fluid particle lies at $z_f = D$, the partition function of the fully atomistic system can be evaluated as

DOI: 10.1021/acs.langmuir.9b00440
Langmuir 2019, 35, 5975−5986

$$Q_{\text{full}}(z_f = D) = \frac{1}{\Lambda^3}\iint \exp\left(-\frac{U_{sf}^{\text{full}}(\mathbf{r}_s^{N_s}, x_f, y_f, z_f = D)}{k_B T}\right) \times dx_f\, dy_f = \frac{A_{\text{full}}}{\Lambda^3}\left\langle \exp\left(-\frac{U_{sf}^{\text{full}}(z_f = D)}{k_B T}\right)\right\rangle_{\{x_f, y_f\}} \quad (6)$$

where A_{full} is the planar area of the simulation box in x- and y-directions, and for a fixed simulation box size, A_{full} is a constant; the angular bracket denotes the ensemble average over all possible x_f and y_f positions with fluid particle fixed at $z_f = D$. Similarly, we can write out a partition function for the corresponding coarse-grained (CG) system shown in Figure 1c as

$$Q_{CG} = \frac{1}{\Lambda^3}\int \exp\left(-\frac{U_{sf}^{\text{AW-FEA}}(\mathbf{r}_f)}{k_B T}\right)d\mathbf{r}_f = \frac{1}{\Lambda^3}\iiint \exp\left(-\frac{\phi_{\text{Hard}}(x_f, z_f) + \phi_{\text{AW-FEA}}(z_f)}{k_B T}\right) \times dx_f dy_f dz_f \quad (7)$$

If eq 7 is evaluated at $z_f = D$, it follows that

$$Q_{CG}(z_f = D) = \frac{1}{\Lambda^3}\exp\left(-\frac{\phi_{\text{AW-FEA}}(z_f = D)}{k_B T}\right) \times \int \exp\left(-\frac{\phi_{\text{Hard}}(x_f, z_f = D)}{k_B T}\right)dx_f \int dy_f \quad (8)$$

We notice that, in our new 2D surface model (Figure 1c), due to the existence of the 2D hard wall, the accessible area to the center of mass of the fluid particle at a specific z-position is restricted. Carrying out the integration in eq 8, we obtain

$$Q_{CG}(z_f = D) = \frac{A_{CG}(z_f = D)}{\Lambda^3}\exp\left(-\frac{\phi_{\text{AW-FEA}}(z_f = D)}{k_B T}\right) \quad (9)$$

where $A_{CG}(z_f) = 2L_a L_y$ is the accessible area in the xy-plane and is a function of the z-position of the fluid particle; L_y is the simulation box length in the y-direction.

The mapping between the atomistic model and the coarse-grained model follows by equating the free energy (i.e., partition function) of both systems (eqs 6 and 9), and for an arbitrary z_f value, it gives[23]

$$Q_{CG}(z_f) = Q_{\text{full}}(z_f) \quad (10)$$

If we further assume a simulation box with box length L_x in the x-direction, eq 10 leads to the equation for the effective AW-FEA solid–fluid potential compatible with the new 2D coarse-grained surface model

$$\frac{\phi_{\text{AW-FEA}}(z_f)}{k_B} = -T \ln\left[\frac{1}{\eta(z_f)}\left\langle \exp\left(-\frac{U_{sf}^{\text{full}}(z_f)}{k_B T}\right)\right\rangle_{\{x_f, y_f\}}\right] \quad (11)$$

where the accessible area fraction is

$$\eta(z_f) = \frac{A_{CG}(z_f)}{A_{\text{full}}} = \frac{2L_a(z_f)L_y}{L_x L_y} = \frac{2L_a(z_f)}{L_x} \quad (12)$$

where the accessible length parameter L_a depends on the z-position of the fluid particle. If the full substrate is simply mapped to a structureless solid with a perfectly flat surface, considered as in Figure 1b, $\eta = 1$ remains the same across the whole system, then eq 11 reduces to the original FEA potential form[23]

$$\frac{\phi_{\text{FEA}}(z_f)}{k_B} = -T \ln\left\langle \exp\left(-\frac{U_{sf}^{\text{full}}(z_f)}{k_B T}\right)\right\rangle_{\{x_f, y_f\}} \quad (13)$$

Area-Weighted Free-Energy Averaging Procedure. In this section, we will discuss the procedures to obtain the accessible area fraction η, accessible length L_a, and the AW-FEA solid–fluid potential, $\phi_{\text{AW-FEA}}$, for the new 2D surface model described in Figure 1c.

Following eq 11, we first need to determine the accessible area fraction η as a function of the z-position of the test fluid particle. From the physical perspective, the parameter η depicts the fraction of accessible area to the center of mass of the test fluid particle with respect to the whole xy-plane. For a specified solid model, we can compute this accessible area fraction η by performing a series of brute force Monte Carlo simulations. In each individual simulation, a single test fluid particle is iteratively placed at a random position on the xy-plane but with a fixed vertical distance to the basal plane. After each random placement of the test particle, the center-of-mass distance between the test particle and all solid atoms will be calculated. When any center-of-mass distance is smaller than a preset minimum distance r_{min}, the test particle overlaps with the solid (inaccessible); otherwise, we count this configuration as a successful attempt (accessible). If each simulation generates a total of N_{config} configurations, among which N_{acc} are counted as successful attempts, the accessible area fraction η at a z-position, $z_f = D$, can be calculated by

$$\eta(z_f = D) = \frac{N_{\text{acc}}}{N_{\text{config}}} \quad (14)$$

From eq 12, the accessible length parameter L_a in the 2D coarse-grained surface model can then be computed by

$$L_a(z_f = D) = \frac{\eta(z_f = D)L_x}{2} = \frac{N_{\text{acc}}L_x}{2N_{\text{config}}} \quad (15)$$

Equations 14 and 15 extract the structural information from the atomistic substrate and map it to that of the corresponding 2D surface model (Figure 1c).

The next step is to extract the energetic information from the "bottom-level" atomistic model. Based on eq 11, a direct route to the effective energetic potential $\phi_{\text{AW-FEA}}$ is from the molecular simulation. Similarly, we carried out a series of simulations, each of which involves a single test fluid particle iteratively being placed at a random position on the xy-plane with a fixed vertical distance $z_f = D$ to the basal plane. The effective potential $\phi_{\text{AW-FEA}}$ is then calculated as an ensemble average

$$\frac{\phi_{\text{AW-FEA}}(z_f = D)}{k_B} = -T \ln\left[\frac{1}{\eta(z_f = D)N_{\text{config}}} \times \sum_{i=1}^{N_{\text{config}}} \exp\left(-\frac{U_{sf}^{\text{full}}(\mathbf{r}_s^{N_s}, x_f, y_f, z_f = D)}{k_B T}\right)\right] \quad (16)$$

DOI: 10.1021/acs.langmuir.9b00440
Langmuir 2019, 35, 5975–5986

where

$$U_{sf}^{full}(\mathbf{r}_s^{N_s}, x_f, y_f, z_f = D) = \sum_{j=1}^{N_s} u(r_{sjf}) = \sum_{j=1}^{N_s} 4\varepsilon_{sf}\left[\left(\frac{\sigma_{sf}}{r_{sjf}}\right)^{12} - \left(\frac{\sigma_{sf}}{r_{sjf}}\right)^{6}\right] \quad (17)$$

where σ_{sf} and ε_{sf} are Lennard-Jones (LJ) size parameter and energy parameter for solid (s)−fluid (f) interaction, respectively; r_{sjf} is the center-of-mass distance between the solid atom j and the single fluid particle. Here, we take the pairwise solid−fluid interaction to have the form of the LJ potential, but in principle, it can be replaced by any other form of the many-body realistic potential to describe the full system.

Averages for both accessible area fraction η and effective potential $\phi_{AW\text{-}FEA}$ were taken over $N_{config} = 10^8$ random configurations for each simulation with a fixed z-position for the single fluid particle. We did not observe a significant difference in the ensemble average when increasing the number of configurations. In the simulations, the relative positions of the fluid-basal plane were discretized using a histogram with a bin size of $0.01\sigma_{ff}$. Periodic boundary conditions were only applied in the x- and y-directions. A cutoff distance $r_c = 5\sigma_{ff}$ was applied to the pairwise Lennard-Jones potential, and the potential was truncated at r_c. The LJ potential parameters for the substrate carbon atoms and argon molecules are listed in Table 1, and the solid−fluid (sf) cross-

Table 1. Lennard-Jones (LJ) Potential Parameters Used in the Monte Carlo Simulations[13,29,30]

	ε/k_B (K)	σ (Å)
C (of substrate)	28.0	3.4
Ar	119.8	3.405
N_2	101.5	3.615

interaction parameters were calculated by the Lorentz−Berthelot combining rules, i.e., $\sigma_{sf} = (\sigma_{ss} + \sigma_{ff})/2$ and $\varepsilon_{sf} = \sqrt{\varepsilon_{ss}\varepsilon_{ff}}$. The simulation box size, 34.43317 Å × 34.08 Å ($L_x \times L_y$), was used to satisfy the periodicity requirement of the graphene structure in the xy-dimension. The box length in the z-dimension was large enough to ensure that the test fluid particle can be elevated to a height where no solid−fluid interactions are present. Forte et al.[23] used a generic Mie potential to fit the discrete effective solid−fluid potential, but in the case of the defective surface model, the Mie potential cannot result in a satisfactory fitting. Therefore, in this work, we used the numerical values of the potential $\phi_{AW\text{-}FEA}$ and accessible length parameter L_a and applied linear interpolation to evaluate the missing data.

Grand Canonical Monte Carlo Simulation. Grand canonical Monte Carlo (GCMC) simulations[27] were carried out to test the new 2D surface model for geometrically heterogeneous surfaces. The number and positions of substrate atoms, the chemical potential of adsorbates, the accessible volume of the system, and temperature were fixed in the simulation. The simulation box dimension, 34.43317 Å × 34.08 Å ($L_x \times L_y$), was used in both the full simulation and the corresponding CG simulation for convenience, but in principle, the box size of the CG simulation does not depend on that of the full simulation. A slit-like pore geometry was used to model the solid substrate. Two symmetric solid blocks were placed at both ends of the simulation box in the z-direction, and the separation between those two substrates was large enough to model the adsorption on two independent open surfaces. Periodic boundary conditions were applied in the x- and y-directions. Solid−fluid interactions in the atomistic system and fluid−fluid interactions were modeled by the standard 12−6 Lennard-Jones potential, and a cutoff radius $r_c = 5\sigma_{ff}$ was chosen. Lennard-Jones parameters required in simulations are listed in Table 1, and cross-interaction terms were calculated from the Lorentz−Berthelot combining rules. Each GCMC simulation consisted of $(2-5) \times 10^7$ moves for equilibrium. The statistics were sampled from the following $(2-5) \times 10^7$ production moves. For the state points that are close to the saturation pressure, at least two independent runs were performed, and the excess adsorption amounts were averaged from these independent runs. The probabilities of making a displacement, an insertion, and a deletion of an adsorbate molecule were set to 0.9, 0.05, and 0.05, respectively. The production stage was divided into blocks, each of which consisted of 1×10^5 MC steps, and standard deviations were calculated from these blocks. Chemical potentials of Ar and N_2 at 87.3 and 77 K were obtained by the Widom insertion method[28] in isothermal−isobaric (NPT) Monte Carlo simulations.

RESULTS AND DISCUSSION

The new 2D surface model can be constructed for any solid substrate with a geometrically heterogeneous surface. We particularly chose Cabot BP-280, a nonporous, nongraphitized activated carbon material,[31] here as one illustrative example to show the superiority of our 2D surface model over the conventional 1D surface model. Cabot BP-280 is commonly used as a reference material representing a wide range of partially graphitized active carbon materials. Scientists usually fit the potential parameters in their DFT method[6−9] and molecular simulation models[29] to the experimental BP-280 data to get some sense of how well their model can represent a real defective activated carbon surface. Here, we modeled BP-280 as a collection of two perfect graphene sheets and a nongraphitized surface with ABA stacking pattern. The spacing between two adjacent graphene layers was 3.35 Å. The degree of geometric defects on the top layer was controlled by two parameters: the percentage of defects, P_d, and the effective defect radius, R_c. To create the defects, we randomly selected a carbon atom on the top layer and then removed it as well as its surrounding atoms within an effective defect radius R_c from the selected atom. The deletion move was repeated until the percentage of removed atoms reached the percentage of defect P_d. More details can be found in ref 1. The excess adsorption on the surface was calculated by

$$\Gamma = \frac{\langle N_f \rangle - V\rho_{bulk}}{S} \quad (18)$$

where angular bracket denotes the ensemble average, V is the accessible volume for adsorbates, ρ_{bulk} is the bulk density of adsorbate molecules at pressure P, and S is the surface area, which was measured by the computational BET method.[1]

To build an atomistic model of BP-280, we computed the adsorption isotherms of Lennard-Jones (LJ) argon at 87.3 K onto the solid substrate model with various combinations of P_d and R_c by GCMC simulations and tentatively selected several

DOI: 10.1021/acs.langmuir.9b00440
Langmuir 2019, 35, 5975−5986

promising adsorption isotherms against the experimental BP-280 data.[32] To further decide the best one, we need an accurate surface area of each model to convert units of the simulation results to that of the experimental data. We performed a series of GCMC adsorption simulations of N_2 at 77 K, and good linearity was found at the relative pressure range from 0.07 to 0.25, which is similar to the relative pressure range (0.06−0.25) in the experimental determination of BET surface area of Cabot BP-280.[31] A cross-sectional area of nitrogen molecule of 16.2 Å^2 was used to calculate the total area of the modeled surface.[1,32] Finally, we picked one surface model that gives the best agreement with the experimental data (see Figure 2a), and the corresponding parameters for the top

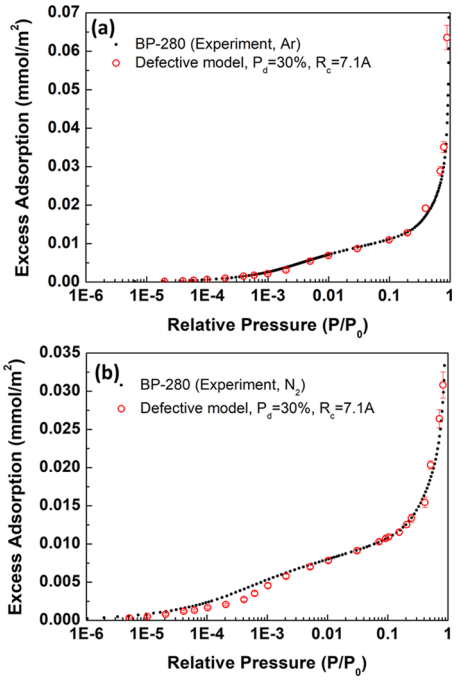

Figure 2. Comparison of simulated adsorption isotherms of (a) Ar at 87.3 K and (b) N_2 at 77 K on BP-280 surface model (with P_d = 30% and R_c = 7.1 Å for the top defective layer) with experimental data.[31,32] P_0 is the bulk-phase saturation pressure. The specific surface area of 40.2 m^2/g[31] was used to convert the experimental volumetric data.

defective layer are P_d = 30% and R_c = 7.1 Å. The percentage of defects in our infinite BP-280 surface model is very close to that of P_d = 29% obtained in the finite surface model.[29] The computational BET method shows that the surface area for the current atomistic model of BP-280 (with P_d = 30% and R_c = 7.1 Å) is 1317.14 Å^2, which is about 12.2% greater than that of the perfect graphene surface ($L_x \times L_y$ = 1173.48 Å^2). To check the independence of the constructed BP-280 surface model on the adsorbate and temperature, we also compared the simulated excess adsorption of N_2 at 77 K against the available experimental BP-280 data.[31] Figure 2b shows a quantitative agreement between the simulated N_2 adsorption data and the experimental BP-280 data over a wide range of pressure considered. We did not attempt to do an exhaustive search of any possible combination of P_d and R_c, but the simulation results in Figure 2 confirm the independence of the current model on the adsorbates and temperature and give us confidence in the physical significance of the chosen parameters. The configuration of the geometrically heterogeneous surface model representing BP-280 is shown in Figure 3a. It should be noted that the method used here to construct

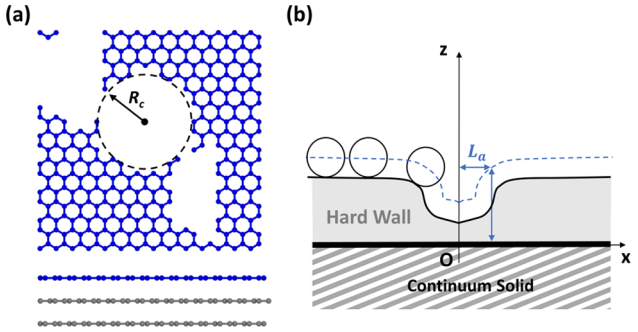

Figure 3. Configuration of the Cabot BP-280 model with P_d = 30% and R_c = 7.1 Å for the top defective layer. (a) Snapshot of the side view of the atomistic substrate (bottom) with top defective layer colored in blue (top). Carbon atoms are drawn to reduced scale for clarity. (b) Corresponding 2D surface model for the BP-280 solid. The boundary of the hard wall is quantitatively drawn based on the MC simulation results of the accessible length L_a. Blue dashed line is the trace of the center of mass of argon molecules (white particles) while rolling over the surface.

the atomistic surface model[1] is not robust in the low-pressure region. We have run adsorption simulations on the other three defective surface samples in addition to the current one with the same P_d and R_c parameters. The adsorption isotherms agree perfectly in the high-pressure region but differ slightly at the low-pressure region ($P/P_0 \lesssim 1 \times 10^{-3}$); such deviations at low pressures result from the random nature of the algorithm in constructing the surface vacancies. Because we will use the same model for both the full system and the coarse-grained system, the deficiency in the construction of the atomistic surface model does not interfere with the validation of our coarse-grained models. In the interests of robustness and reproducibility, a more sophisticated atomistic surface model is desired in the future.

Now, we follow the procedure to construct a 2D surface model for the atomic BP-280 solid. Unless otherwise stated, all of the following simulations are for the adsorption of argon onto the surface at 87.3 K. Here, we assume that the position of the basal plane (i.e., z = 0) in the coarse-grained system corresponds to that of the second graphene layer in the full system. For the calculation of accessible area fraction η, a minimum distance of r_{min} = 3.4025 Å was used; the choice of this specific value is based on the Lorentz combining rule, $\sigma_{sf} = (\sigma_{ss} + \sigma_{ff})/2$, of the LJ size parameter for the carbon atom (σ_{ss} = 3.4 Å) and for the argon particle (σ_{ff} = 3.405 Å). Once the structural information of the atomic BP-280 model is obtained from eqs 14 and 15, we can construct the corresponding 2D surface model shown in Figure 3b. The boundary of the hard wall is quantitatively drawn based on the simulation results of the accessible length parameter L_a (numerical data of η and L_a are available in Tables S1 and S2, respectively). As expected, when z_f is very small, $\eta \sim 0$ and $L_a \sim 0$ Å. As the position of the fluid particle is commensurate to that of the vacancies in the top layer, fluid particles can fit into those pits, but the accessible area in the pit is restricted due to the strong repulsion between the fluid particle and the solid atoms. When the fluid particle is elevated high enough away from the surface, the accessible area at that z-position becomes the whole xy-plane, thus η = 1; following eq 15, the accessible

DOI: 10.1021/acs.langmuir.9b00440
Langmuir 2019, 35, 5975−5986

length L_a now equals half of the simulation box length L_x in the x-direction, and the shape of the hard wall flattens. We also calculated the geometric surface area of the corrugated hard wall (i.e., the Connolly surface area), and it was about 1382 Å^2, very close to the computational BET surface area of the atomistic BP-280 model (1317.14 Å^2). This agreement confirms that the new coarse-graining scheme can reasonably extract the structural information of the surface from the fully atomistic substrate. To be consistent, we used the computational BET surface area of the atomistic model in the calculation of excess adsorption amount for both full simulation and corresponding coarse-grained simulation.

After getting the accessible area fraction η, we can numerically calculate the area-weighted (AW) energetic potential $\phi_{AW\text{-}FEA}$ by carrying out brute force Monte Carlo simulations following eq 16. Figure 4 shows the potential

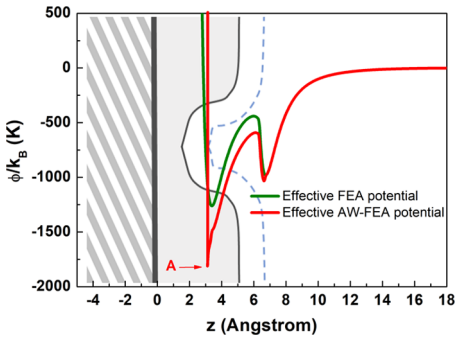

Figure 4. Comparison between the effective AW-FEA potential (red curve), $\phi_{AW\text{-}FEA}$, for the 2D surface model and the conventional effective FEA potential (green curve), ϕ_{FEA}, associated with the 1D surface model for the BP-280 solid (P_d = 30% and R_c = 7.1 Å). The adsorbate particle is modeled as LJ argon at 87.3 K. Background 2D coarse-grained model is taken from Figure 3b. Point A indicates the discontinuity in the effective AW-FEA potential.

$\phi_{AW\text{-}FEA}$ as the energetic part of the total solid−fluid potential for the 2D surface model representing the BP-280 solid. The conventional free-energy-averaged (FEA) potential ϕ_{FEA} of eq 13 is also plotted in the figure for comparison. Both the FEA and AW-FEA potentials show two potential minima over the full range. The first potential minimum ($z \sim 3$ Å) is due to the strong attraction of the active vacancies in the surface and the second potential minimum ($z \sim 6.5$ Å) arises from the contribution from the whole solid substrate, and its position corresponds to the center-of-mass position of a fluid particle lying on the flat surface (see the blue dashed line in Figure 4). When the fluid particle is close to the surface, it can feel the strong attractions from the active vacancies, and $\eta < 1$ leads to a deeper first potential minimum for $\phi_{AW\text{-}FEA}$ than that for the conventional FEA potential. At large distance from the surface, the accessible area fraction η is close to 1 and it has little impact on the shape of the potential; thus, the second minimum overlaps for both potentials. In the 2D surface model, there is a 2D hard wall above the background continuum solid. When the fluid particle overlaps with the hard wall, the potential $\phi_{AW\text{-}FEA}$ goes to infinity, which results in a discontinuity at the first potential minimum (see point "A" in Figure 4). Numerical data of $\phi_{AW\text{-}FEA}$ for the 2D surface model representing the BP-280 solid are stored in the "cg_wall.txt" file in the Supporting Information.

To further validate our new 2D surface model, we computed the excess adsorption isotherms for argon at 87.3 K on the Cabot BP-280 solid. The comparison among the fully atomistic model and the new 2D surface model with the effective AW-FEA potential and the conventional 1D surface model with the effective FEA potential is shown in Figure 5. The adsorption

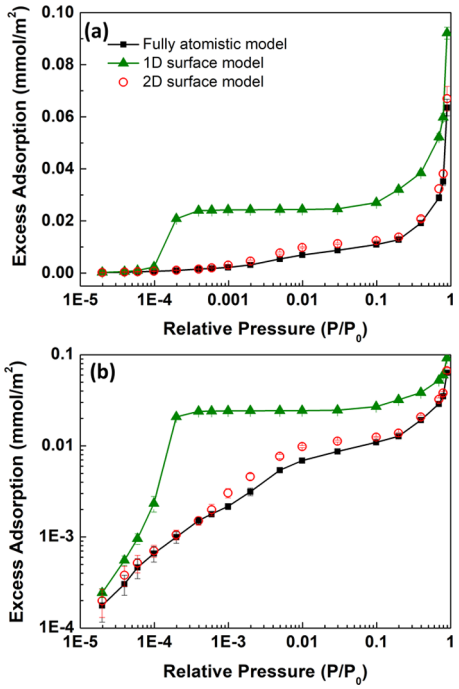

Figure 5. Excess adsorption isotherms of argon at 87.3 K on the BP-280 solid (P_d = 30% and R_c = 7.1 Å) by different surface models. The only difference between (a) and (b) is the use of a logarithmic scale for the y-axis in (b). P_0 is the saturation pressure of bulk-phase argon at 87.3 K.

isotherm by the 2D surface model is in excellent agreement with the full simulation, taking into account the wide range of relative pressure from 1×10^{-5} to 1. The 1D surface model represented by the effective FEA potential, however, is unable to reproduce the correct shape of the adsorption isotherms, and as expected, it overestimates the excess adsorptions more severely than that found in ref 23. In contrast to the adsorption isotherm produced by the 1D surface model, which shows a "step" around the relative pressure of 2×10^{-4} associated with the layering transition on the flat structureless surface, the shape of the adsorption isotherm for the fully atomistic substrate and the 2D surface model is very smooth. The reason for this difference is that the 1D surface model does not allow for the vacancies on the surface and it only describes the adsorption behavior on a perfectly flat surface. For a real heterogeneous surface, the fluid atoms will first adsorb onto the highly active vacancies; once they occupy those vacancies, the adsorption on other surface sites then starts. However, due to the limited number and sizes of the vacancies, there are few fluid particles that can be fitted into the defects. The above argument is further supported by Figure 6 showing the density profile of the fully atomistic model and of the coarse-grained surface model. We can see that the 1D surface model with the effective FEA potential shows prominent first layer adsorption on the flat surface at z = 3−4 Å, which corresponds to the first potential minimum in Figure 4. In comparison, the 2D surface

DOI: 10.1021/acs.langmuir.9b00440
Langmuir 2019, 35, 5975−5986

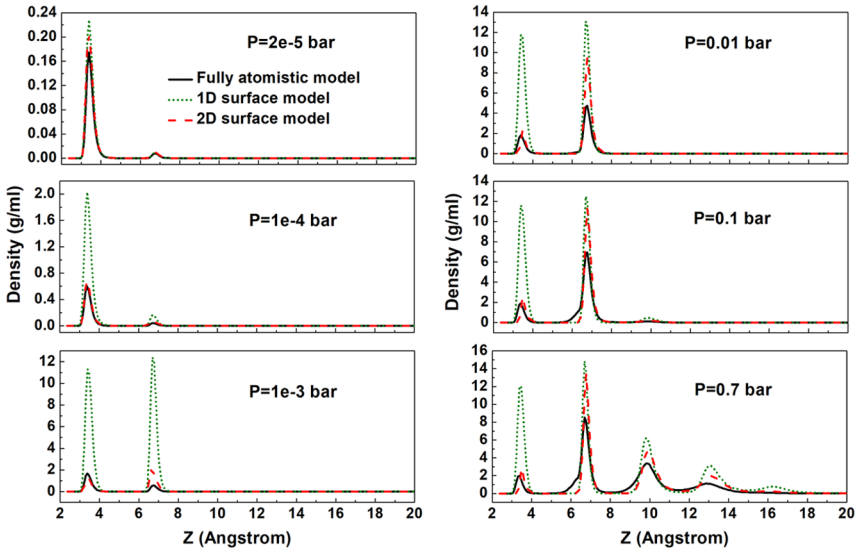

Figure 6. Density profile of the adsorbed argon molecules on the BP-280 solid surface (P_d = 30% and R_c = 7.1 Å) in the z-direction (perpendicular to the surface) by different surface models at 87.3 K.

model with the AW-FEA potential allowing for the geometric defects on the surface reproduces the same and correct first layer adsorption in geometric vacancies as in the full model, which indicates that the addition of one more dimension to the coarse-grained surface model and the introduction of the accessible area fraction η to the traditional free-energy-averaged scheme are essential to predict the correct adsorption behavior on the geometrically heterogeneous surfaces.

Despite the overall improvement in the predictive quality of the adsorption isotherm and density profile by the 2D surface model, it still overestimates the excess adsorption at the middle-pressure range, i.e., from the relative pressure of 0.001−0.01. Figure 6 also indicates this overestimation in the second adsorbed layer around z = 6−7 Å associated with the adsorption on the outer surface (corresponding to the second potential minimum in Figure 4). The inaccuracy over this pressure range originates from the intrinsic deficiency of the 1D AW-FEA potential, $\phi_{AW\text{-}FEA}$. As illustrated in Figure 7, due to the existence of the surface vacancies, the adsorption energy across the outer surface is heterogeneous for the real atomistic model, showing strong attraction on perfect lattice sites and weak attraction near the defected lattice site (vacancies). Such heterogeneity leads to the anisotropic density distribution of the particles on the outer surface. For the 2D surface model, however, the effective potential $\phi_{AW\text{-}FEA}$ shows the energetic variation only in the z-direction and assumes energetic homogeneity in the other two directions (x- and y-directions), thus generating a uniform distribution of the fluid particles across the outer surface. Adding one more dimension to the effective potential $\phi_{AW\text{-}FEA}$ in the x- or y-direction would possibly solve this discrepancy but with a higher computational expense.

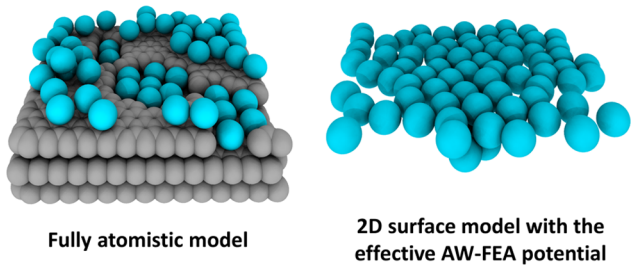

Figure 7. Snapshots of the argon (cyan particles) adsorbed on the fully atomistic BP-280 solid surface (in gray color, P_d = 30% and R_c = 7.1 Å) and on the new 2D coarse-grained surface model at a bulk pressure of 0.01 bar, 87.3 K, showing the energetic heterogeneity of the full potential across the outer surface exerted by the atomistic substrate (left figure) and the energetic homogeneity of the 1D effective solid−fluid potential $\phi_{AW\text{-}FEA}$ in directions parallel to the outer surface (right figure). For the 2D surface model, the structureless wall below the adsorbed layer is not shown.

To confirm the universal applicability of our new 2D surface model, we tested another three nongraphitized graphitic solids with the top defective surface having P_d of 5, 30, and 50% and R_c of 2.84, 5.68, and 8.5 Å. Figure 8 summarizes these three testing cases and includes snapshots of the top defective layer, corresponding 2D coarse-grained surface model, comparison between the effective AW-FEA potential, $\phi_{AW\text{-}FEA}$ of eq 11, with the traditional FEA potential, ϕ_{FEA} of eq 13, and excess adsorption isotherms by different surface models. From the left to the right column, the combination of P_d and R_c indicates the increment of the geometric roughness of the top surface. Accordingly, the size of the geometric vacancy in the 2D surface model also increases, confirming again that the 2D surface model can extract the important structural information from its atomistic counterpart. Looking at the shape of the potentials, when the level of roughness is low (P_d = 5% and R_c = 2.84 Å), the potential $\phi_{AW\text{-}FEA}$ exhibits distinct differences in both shape and minimum values from the conventional FEA potential near the first potential minimum, and such differences in the potential are reflected by the large discrepancies in the excess adsorption isotherms. As the roughness of the top surface increases, the shape of the AW-FEA and FEA potentials becomes more similar but still differs in the first potential minimum due to the introduction of parameter η into the AW-FEA potential. The deeper first minimum in $\phi_{AW\text{-}FEA}$ ensures the correct adsorption amount at extremely low pressures. Over the middle-pressure range (0.001−0.01), deviations in adsorption isotherms between the 2D surface model and the fully atomistic model are observed again and get worse with higher levels of surface roughness.

DOI: 10.1021/acs.langmuir.9b00440
Langmuir 2019, 35, 5975−5986

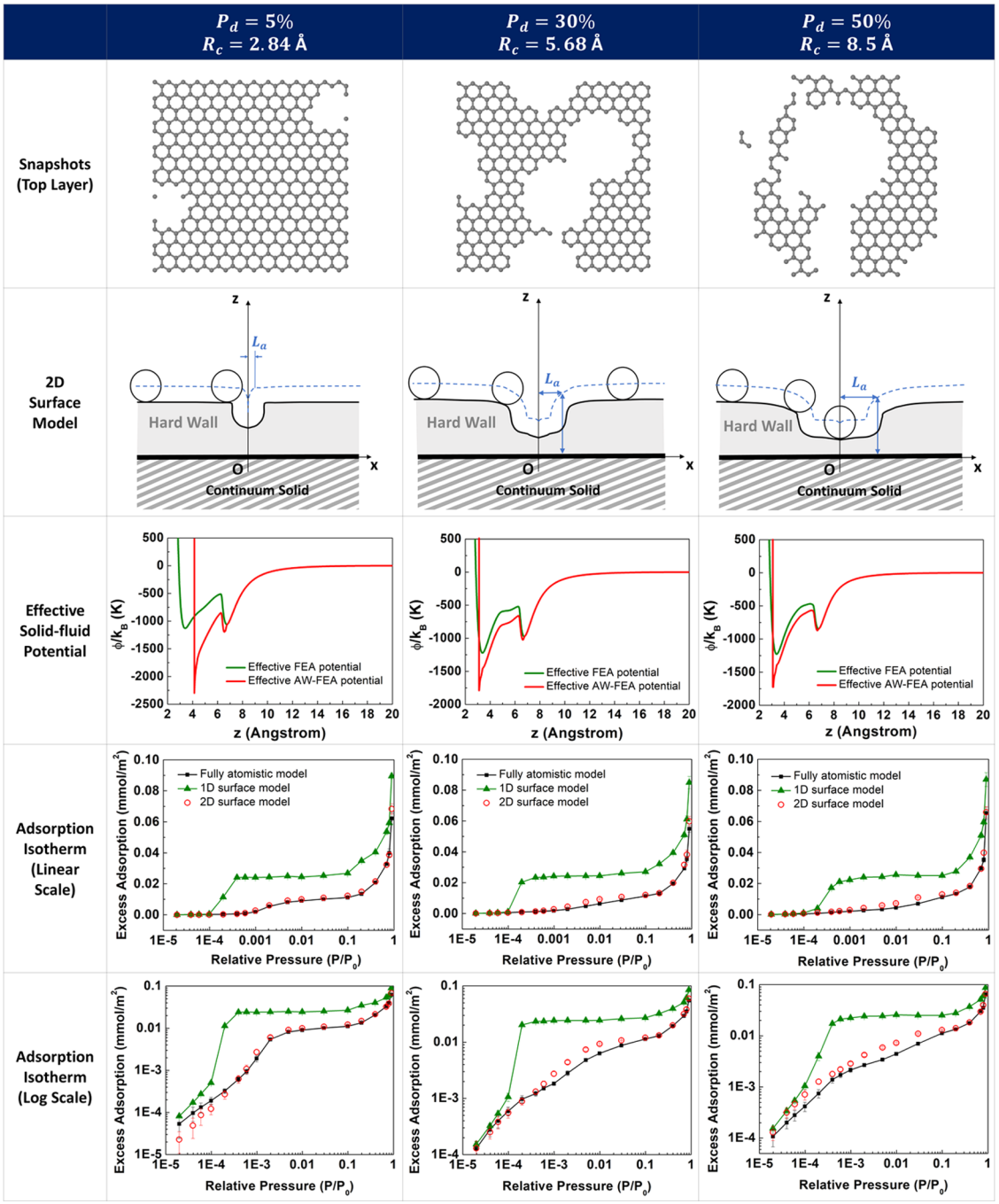

Figure 8. Application of the new 2D surface model based on the effective AW-FEA potential to three nongraphitized surfaces with different levels of roughness. The 2D surface models are drawn in the same way as in Figure 3b. See the text for details.

The reason is that when the surface becomes more defective, the energetic heterogeneity gets more distinct for the perfect lattice site and the defective vacancies, and the 1D potential $\phi_{\text{AW-FEA}}$ deviates more from the real situation. In general, the 2D surface model significantly improves the overall accuracy of the predicted adsorption isotherm over the traditional 1D surface model, which is based on the original FEA potential.

CONCLUSIONS

In this study, we present a bottom-up strategy to construct the coarse-grained (CG) surface model and the corresponding effective solid−fluid potential with a low-dimensional positional dependence for a heterogeneous surface substrate. Instead of fitting the model parameters to the top-level experimental adsorption data as the traditional top-down method, the bottom-up strategy is based upon obtaining the coarse-grained parameters directly from the bottom-level atomic model.

Specifically, for the solid substrate with a geometrically heterogeneous surface, we proposed a numerical method to construct a corresponding two-dimensional (2D) coarse-grained surface model. The total potential model is composed of two parts: the structural part is a 2D hard wall potential representing the geometric defects in the atomistic heterogeneous surface, and the energetic part is a 1D effective area-weighted free-energy-averaged (AW-FEA) potential representing the solid−fluid interactions averaged over the directions

DOI: 10.1021/acs.langmuir.9b00440
Langmuir 2019, 35, 5975−5986

parallel to the surface at a certain z-distance. In the computation of the effective AW-FEA potential, the free energy of the full system is mapped to the free energy of the coarse-grained system containing a 2D surface model. A new parameter η containing the accessible area information for the fluid particle close to the surface naturally appears; the introduction of this surface-structure-related parameter allows us to incorporate the structural dependence into the effective solid−fluid potential on the atomistic substrate. By using the new AW-FEA scheme, an accurate but coarse-grained representation of any defective atomistic surface model can be established without being restricted by the defective crystalline structure of the solid substrate, as is the original free-energy-averaged method.[23] Monte Carlo simulations were carried out to get basic parameters for the new 2D surface model from the fully atomistic substrate. The simulation results show that the hard wall configuration in the new 2D surface model retains the structural details from the full system. Grand canonical Monte Carlo simulations were performed for the argon adsorption onto a widely used reference nongraphitic substrate, BP-280, to test the validity of the 2D surface model against the fully atomistic system. The simulation results indicate that adding one more dimension to the conventional 1D surface model based on the effective FEA potential is essential to reproduce the correct adsorption behavior with minimal increase of the computational expense; in particular, the 2D surface model significantly improves the adsorption isotherm and density profile compared to the traditional 1D surface model over a wide range of pressure. The further test of another three nongraphitized substrates with different levels of geometric roughness for the top layer confirms the effectiveness and accuracy of the new 2D surface model. We found that despite the mostly quantitative agreement of the adsorption isotherm between the fully atomistic model and the 2D surface model, the latter still slightly overestimates the adsorption amount over a middle-pressure range. This is believed to be an intrinsic deficiency of the 1D effective AW-FEA potential, where the energetic variation is present only in the direction perpendicular to the surface while being energetically homogeneous in the other two directions. This overestimation might be solved by introducing another dimension (degree of freedom) into the 1D AW-FEA potential.

Although we consider only the geometrically heterogeneous surface case, here, we believe that this bottom-up strategy could also be developed to deal with energetically heterogeneous surfaces. To account for the surface energetic sites, it should be possible to apply the conformal sites theory[4] to simplify the current analytical solid−fluid potential. The conformal sites theory states that an energetically heterogeneous real surface can be mapped to an energetically homogeneous reference surface. We briefly outline such an approach in the Appendix and plan to develop this further in future work. During the preparation of this manuscript, we became aware of an independent work on the development of coarse-grained solid−fluid potentials for heterogeneous surfaces that has been carried out by Ravipati et al.[33] Interested readers should refer to their work for more details.

As for current software embedded in experimental sorptometers, simulation results are precalculated and stored in the software. As computing power increases, it will be possible to run real-time coarse-grained simulations and theoretical calculations (e.g., density functional theory) on personal computers. An accurate, flexible but simple potential is essential in getting reliable data on time. The use of the CG surface model and its compatible effective solid−fluid potential will enable faster execution in computer simulations and easier manipulation in theories.

APPENDIX

Coarse-Grained Description of Solid−Fluid Interactions for Energetically Heterogeneous Surface Model

On most real surfaces, there are not only geometrical defects but also energetic heterogeneities due to chemical composition, impurities, and functional groups attached or deposited onto the surface. An effective or analytical expression for the solid−fluid potential is desirable for such anisotropic interactions of adsorbate molecules with energetically heterogeneous surfaces. However, due to so many potential parameters for different energetic sites on the surface, the traditional direct integration is impossible to perform. Theoretical attempts have been made in the DFT method[8,11] and in statistical associating fluids theory[34] to account for the energetically heterogeneous surface, but again, these approaches require fitting model parameters to the top-level experimental data and have limited connections to the "atomic-level" substrate. Recently, we developed a conformal sites theory,[4] stating that a real interfacial system with an energetically heterogeneous surface can be mapped onto a reference system with an energetically homogeneous surface. Such a mapping process is realized by doing the perturbation expansion of the free energy of a real system about that for a reference system, and the potential parameters for the reference system are then obtained by annulling the first-order terms in the perturbation expansion. It is shown that the theory can generally give quantitatively good estimates of the surface excess for the adsorption on a highly heterogeneous surface even when the surface sites differ in LJ energy parameters by a factor of 5, in LJ size parameter by a factor of 1.1, and in partial charge by a factor of 3−10 depending on the type of molecules.[4] The conformal sites theory can simplify the theoretical treatment of the energetically heterogeneous surfaces and provide a flexible and accurate way to account for solid−fluid interactions. If we assume a solid substrate with a geometrically uniform surface made up of different adsorption sites, of species α, β, ..., among which are included the main composition of the solid substrate (s); these heterogeneous sites are assumed to be present only on the surface of the solid substrate and interact with fluid particles through Lennard-Jones interactions. By applying the conformal sites theory to the conventional 1D coarse-grained model shown in Figure 1b, we can write out an effective solid−fluid potential ϕ_{sf} in a general form[8] for the adsorption of pure fluids on such an energetically heterogeneous surface model

$$\phi_{sf}(z_f) = \phi_1(z_f) + \phi_\infty(z_f) \tag{A1}$$

where the first term ϕ_1 on the right is the potential of interaction with the energetic surface and ϕ_∞ is the potential of interaction with the rest of the solid.

Specifically, if we presume the solid substrate to be a graphitic substrate with a geometrically perfect but energetically heterogeneous surface, these potentials can then be formulated in the form of 10-4-3 Steele potential[8,13]

DOI: 10.1021/acs.langmuir.9b00440
Langmuir 2019, 35, 5975−5986

$$\phi_1(z_f) = 2\pi\rho_s\varepsilon_x\sigma_x^2\Delta\left[\frac{2}{5}\left(\frac{\sigma_x}{z_f}\right)^{10} - \left(\frac{\sigma_x}{z_f}\right)^4\right] \quad \text{(A2)}$$

$$\phi_\infty(z_f) = -\frac{2\pi\rho_s\varepsilon_{sf}\sigma_{sf}^6}{3(z_f + 0.61\Delta)^3} \quad \text{(A3)}$$

where z_f is the distance of a fluid particle from the graphite surface, ρ_s is the density of carbon atoms in graphite (ρ_s = 0.114 Å^{-3}), and Δ is the spacing between two adjacent graphene layers (Δ = 3.35 Å). The solid−fluid (sf) energy parameter ε_{sf} and size parameter σ_{sf} are calculated from the Lorentz−Berthelot combining rules. The reference solid−fluid energy parameter ε_x and size parameter σ_x represent the average energy parameter and size parameter, respectively, for a fluid particle interacting with the main surface atoms and various energetic adsorption sites on the surface. They can be calculated by[4]

$$\varepsilon_x = \frac{\sum_\alpha x_\alpha\varepsilon_{\alpha f}\sigma_{\alpha f}^3}{\sum_\alpha x_\alpha\sigma_{\alpha f}^3} \quad \text{(A4)}$$

$$\sigma_x = \left(\frac{\sum_\alpha x_\alpha\sigma_{\alpha f}^3}{\sum_\alpha x_\alpha}\right)^{1/3} \quad \text{(A5)}$$

where x_α is the mole fraction of the surface sites of species α; $\varepsilon_{\alpha f}$ and $\sigma_{\alpha f}$ are the LJ energy parameter and size parameter, respectively, for the pair of the surface site of species α and pure fluid particle (f). Summations are over all types of the surface sites. Once we know the mass/mole fractions of each surface site type from experiments (e.g., XPS), we can calculate conformal sites parameters ε_x and σ_x and hence construct an effective potential (eq A1) for such an energetically heterogeneous surface. It is also possible to construct an analytical solid−fluid potential for an energetically heterogeneous surface with well-defined geometric defects. In that case, it is necessary to introduce another degree of freedom (either in the x-direction or in y-direction) to eq A1. Examples are surface defects of a saw-toothed profile with a rectangular shape,[14,15] triangular shape (stepped surface),[16] and trigonometric function shape.[8] In the case where energetic sites only are distributed on the partial surface or are localized in an area, the derivation of such an analytical potential requires the integration over part of the surface, and the total solid−fluid potential is just a linear combination of each contributing part.

■ ASSOCIATED CONTENT

Supporting Information

The Supporting Information is available free of charge on the ACS Publications website at DOI: 10.1021/acs.langmuir.9b00440.

Numerical structural input parameters for the 2D surface model representing the BP-280 solid (PDF)

Numerical 1D effective area-weighted free-energy-averaged (AW-FEA) solid−fluid potential for the 2D surface model representing the BP-280 solid (TXT)

■ AUTHOR INFORMATION

Corresponding Authors

*E-mail: eesantis@ncsu.edu (E.E.S.).

*E-mail: keg@ncsu.edu (K.E.S.).

ORCID

Kaihang Shi: 0000-0002-0297-1746

Keith E. Gubbins: 0000-0001-6760-5897

Notes

The authors declare no competing financial interest.

■ ACKNOWLEDGMENTS

The authors thank Dr. Srikanth Ravipati and Prof. Qing Shao for helpful discussions. The authors also thank the U.S. National Science Foundation for support of this research under grant no. CBET-1603851.

■ REFERENCES

(1) Do, D. D.; Do, H. D. Modeling of Adsorption on Non-graphitized Carbon Surface: GCMC Simulation Studies and Comparison with Experimental Data. *J. Phys. Chem. B* **2006**, *110*, 17531−17538.

(2) Seaton, N. A.; Friedman, S. P.; MacElroy, J. M. D.; Murphy, B. J. The Molecular Sieving Mechanism in Carbon Molecular Sieves: A Molecular Dynamics and Critical Path Analysis. *Langmuir* **1997**, *13*, 1199−1204.

(3) Lucena, S. M.; Paiva, C. A. S.; Silvino, P. F.; Azevedo, D. C.; Cavalcante, C. L. The effect of heterogeneity in the randomly etched graphite model for carbon pore size characterization. *Carbon* **2010**, *48*, 2554−2565.

(4) Shi, K.; Santiso, E. E.; Gubbins, K. E. Conformal sites theory for adsorbed films on energetically heterogeneous surfaces, to be submitted.

(5) Wongkoblap, A.; Do, D. D. The effects of energy sites on adsorption of Lennard−Jones fluids and phase transition in carbon slit pore of finite length a computer simulation study. *J. Colloid Interface Sci.* **2006**, *297*, 1−9.

(6) Ustinov, E. A.; Do, D. D.; Fenelonov, V. B. Pore size distribution analysis of activated carbons: Application of density functional theory using nongraphitized carbon black as a reference system. *Carbon* **2006**, *44*, 653−663.

(7) Neimark, A. V.; Lin, Y.; Ravikovitch, P. I.; Thommes, M. Quenched solid density functional theory and pore size analysis of micro-mesoporous carbons. *Carbon* **2009**, *47*, 1617−1628.

(8) Jagiello, J.; Olivier, J. P. 2D-NLDFT adsorption models for carbon slit-shaped pores with surface energetical heterogeneity and geometrical corrugation. *Carbon* **2013**, *55*, 70−80.

(9) Aslyamov, T.; Khlyupin, A. Density functional theory formulation for fluid adsorption on correlated random surfaces. *J. Chem. Phys.* **2017**, *147*, No. 154703.

(10) Ravikovitch, P. I.; Neimark, A. V. Density Functional Theory Model of Adsorption on Amorphous and Microporous Silica Materials. *Langmuir* **2006**, *22*, 11171−11179.

(11) Jagiello, J.; Olivier, J. P. Carbon slit pore model incorporating surface energetical heterogeneity and geometrical corrugation. *Adsorption* **2013**, *19*, 777−783.

(12) Crowell, A. D.; Steele, R. B. Interaction Potentials of Simple Nonpolar Molecules with Graphite. *J. Chem. Phys.* **1961**, *34*, 1347−1349.

(13) Steele, W. A. The physical interaction of gases with crystalline solids. *Surf. Sci.* **1973**, *36*, 317−352.

(14) Bojan, M. J.; Steele, W. A. Computer simulation of physisorption on a heterogeneous surface. *Surf. Sci.* **1988**, *199*, L395−L402.

(15) Bojan, M. J.; Steele, W. A. Computer simulation of physisorbed krypton on a heterogeneous surface. *Langmuir* **1989**, *5*, 625−633.

(16) Bojan, M. J.; Steele, W. A. Computer simulation of physical adsorption on stepped surfaces. *Langmuir* **1993**, *9*, 2569−2575.

(17) Zhao, X.; Johnson, J. K. An Effective Potential for Adsorption of Polar Molecules on Graphite. *Mol. Simul.* **2005**, *31*, 1−10.

DOI: 10.1021/acs.langmuir.9b00440
Langmuir 2019, 35, 5975−5986

(18) Siderius, D. W.; Gelb, L. D. Extension of the Steele 10-4-3 potential for adsorption calculations in cylindrical, spherical, and other pore geometries. *J. Chem. Phys.* **2011**, *135*, No. 084703.
(19) Nguyen, P. T. M.; Do, D. D.; Nicholson, D. On The Cavitation and Pore Blocking in Cylindrical Pores with Simple Connectivity. *J. Phys. Chem. B* **2011**, *115*, 12160−12172.
(20) Gor, G. Y.; Rasmussen, C. J.; Neimark, A. V. Capillary Condensation Hysteresis in Overlapping Spherical Pores:A Monte Carlo Simulation Study. *Langmuir* **2012**, *28*, 12100−12107.
(21) Rasmussen, C. J.; Gor, G. Y.; Neimark, A. V. Monte Carlo Simulation of Cavitation in Pores with Nonwetting Defects. *Langmuir* **2012**, *28*, 4702−4711.
(22) Liu, L.; Zeng, Y.; Do, D. D.; Nicholson, D.; Liu, J. Development of averaged solid−fluid potential energies for layers and solids of various geometries and dimensionality. *Adsorption* **2018**, *24*, 1−9.
(23) Forte, E.; Haslam, A. J.; Jackson, G.; Müller, E. A. Effective coarse-grained solid−fluid potentials and their application to model adsorption of fluids on heterogeneous surfaces. *Phys. Chem. Chem. Phys.* **2014**, *16*, 19165−19180.
(24) Barker, J. A. Conformal Solution Theory and Dipole Interaction. *J. Chem. Phys.* **1951**, *19*, 1430.
(25) Gubbins, K. E. The theory of non-electrolyte solutions: an historical review. *Mol. Phys.* **2013**, *111*, 3666−3697.
(26) Khlyupin, A.; Aslyamov, T. Random Process Theory Approach to Geometric Heterogeneous Surfaces: Effective Fluid−Solid Interaction. *J. Stat. Phys.* **2017**, *167*, 1519−1545.
(27) Frenkel, D.; Smit, B. *Understanding Molecular Simulation: From Algorithms to Applications*, 2nd ed.; Academic Press: San Diego, 2002.
(28) Widom, B. Some Topics in the Theory of Fluids. *J. Chem. Phys.* **1963**, *39*, 2808−2812.
(29) Wongkoblap, A.; Do, D. D. Characterization of Cabot non-graphitized carbon blacks with a defective surface model: Adsorption of argon and nitrogen. *Carbon* **2007**, *45*, 1527−1534.
(30) Ravikovitch, P. I.; Vishnyakov, A.; Russo, R.; Neimark, A. V. Unified Approach to Pore Size Characterization of Microporous Carbonaceous Materials from N 2, Ar, and CO 2 Adsorption Isotherms. *Langmuir* **2000**, *16*, 2311−2320.
(31) Kruk, M.; Jaroniec, M.; Gadkaree, K. P. Nitrogen Adsorption Studies of Novel Synthetic Active Carbons. *J. Colloid Interface Sci.* **1997**, *192*, 250−256.
(32) Gardner, L.; Kruk, M.; Jaroniec, M. Reference data for argon adsorption on graphitized and nongraphitized carbon blacks. *J. Phys. Chem. B* **2001**, *105*, 12516−12523.
(33) Ravipati, S.; Galindo, A.; Jackson, G.; Haslam, A. An investigation of free-energy-averaged (coarse- grained) potentials for fluid adsorption on heterogeneous solid surfaces, (personal communication, 2019).
(34) Kern, J.; Johannsen, M. Modeling adsorption on energetically heterogeneous surfaces with an extended SAFT-VR approach. *J. Supercrit. Fluids.* **2018**, *133*, 70−76.

DOI: 10.1021/acs.langmuir.9b00440
Langmuir 2019, 35, 5975−5986